ORIGINAL ARTICLE

Crystal structure and optical properties of a high-density InGaN nanoumbrella array as a white light source without phosphors

Tetsuya Kouno[1], Masaru Sakai[2], Katsumi Kishino[3], Akihiko Kikuchi[3], Naoki Umehara[4] and Kazuhiko Hara[1,4]

We demonstrated the fabrication of a peculiar GaN/InGaN-based high-density nanocrystal array on a nitrogen polarity GaN layer using a simple self-assembly process for the first time. The nanocrystals consist of bending InGaN nanoplates and supporting GaN nanocolumns. The nanocrystals are umbrella shaped with diameters of ~200–700 nm; therefore, they are referred to as InGaN nanoumbrellas. Transmission electron microscopy revealed the crystal structures of the nanoumbrellas and provided information about their growth mechanism. The photoluminescence (PL) properties of the InGaN nanoumbrellas were also characterized, and an extremely wide range of optical emission wavelengths (~360–800 nm) was obtained from a small excitation diameter of ~10 μm. Multiple sharp peaks resembling lasing actions were also observed in the PL spectrum; the resonant mode was likely caused by the whispering gallery mode. These results indicate that the high-density GaN/InGaN-based nanoumbrella array can be used as a source of white light without phosphors.

INTRODUCTION

The characteristics of nitride nanocrystals and their fabrication techniques have been investigated because of their fascinating optical properties of strong light emission compared with planar film crystals owing to the high-quality crystallinity and strain relaxation.[1–3] Traditionally, self-assembled one-dimensional nitride nanocrystals, nanocolumns, nanorods and nanowires have been actively studied.[2–11] However, it is difficult to design optical cavities and obtain stable characteristics for these structures because of the nonuniformity of the nanocrystal configurations. Recently, selective-area growth (SAG) techniques have been developed to overcome such problems. By combining electron beam lithography and ordinary crystal growth techniques (for example, metalorganic chemical vapor deposition and molecular beam epitaxy (MBE)), SAG techniques have successfully produced periodically arranged one-dimensional nanocrystal arrays.[1,12–18] The arrangements and structures of these nitride nanocrystals are designed to act as tiny optical cavities of photonic crystals, ring resonators, and so on. Owing to their high degree of crystallinity and tiny optical cavities, such nitride nanocrystals are expected to be applicable in high-performance light-emitting diodes (LEDs) and laser diodes. The recently developed SAG techniques are excellent methods to design the tiny optical cavities that are required to precisely control the positions and configurations of nitride nanocrystals. However, SAG is often a complex process that could increase the cost of nanocrystal fabrication. Thus, in this study, we

fabricated nanocrystals with unique configurations using a simple self-assembly process. The novel nanocrystals themselves act as optical cavities. Although the optical properties of the nanocrystals are not uniform, we suggest that this nonuniformity can be a significant advantage, namely, it can realize emission in an extremely wide range emission potentially leading to a low-cost white light source.

We previously realized GaN nanodisks via crystal growth without SAG; these nanodisks acted as optical cavities for the whispering gallery mode (WGM).[19] However, the nanodisk density was too low for use in optical devices, and the nanodisks exhibited sharp peaks at only ~370 nm wavelength owing to the optical gain of the GaN crystal. We also realized unique InGaN nanoplates using nitrogen-polarity (N-polarity) GaN templates as substrates along with a lateral growth technique and a SAG technique involving radio frequency-plasma-assisted MBE (RF-MBE).[20] The nanoplates exhibited visible emissions, and their configurations could potentially act as the WGM. However, the fabrication of these nanoplates included a complicated SAG process and the WGM was not actually demonstrated. Thus far, similar structures have been demonstrated for ZnO nanocrystals.[21–23] It was reported that these crystals also acted as optical cavities for the WGM around a wavelength of 390 nm; we consider that these nanocrystals are potential alternatives to optical devices based on the WGM. However, ZnO-based mixed crystals exhibiting emission in the entire visible range have not been demonstrated. In contrast, it is

[1]Department of Electronics and Material Science, Shizuoka University, Hamamatsu, Japan; [2]Interdisciplinary Graduate School of Medicine and Engineering, University of Yamanashi, Kofu, Japan; [3]Department of Engineering and Applied Sciences, Sophia University, Tokyo, Japan and [4]Graduate School of Science and Technology, Shizuoka University, Hamamatsu, Japan
Correspondence: Dr T Kouno, Department of Electronics and Material Science, Shizuoka University, 3-5-1, Johoku, Naka-ku, Hamamatsu-shi, Shizuoka 432-8011, Japan.
E-mail: tetsuya.kouno@gmail.com or kono.tetsuya@shizuoka.ac.jp

generally known that InGaN-based crystals can potentially cover the whole visible range.

In this study, we simplified the growth procedure of previously reported InGaN nanoplates as shown in Kouno and Kishino,[20] and we realized high-density arrays of InGaN-based nanocrystals that have unique configurations like a nanoumbrella. The InGaN-based high-density nanoumbrella array exhibited an extremely wide range of visible emission and highly useful properties for white light sources. In addition, the InGaN-based nanoumbrellas acted as WGM optical nanocavities in their extremely wide range of visible emission. Thus far, there have been no demonstrations of optical nanocavities covering such a wide range of visible light to the best of our knowledge. In our previous study[19] and in other studies that demonstrated III-nitride nanocrystals, the resonant peaks based on optical nanocavities were obtained with a specific range of emission wavelengths. We characterized the InGaN-based nanoumbrella crystal structures using transmission electron microscopy (TEM) and revealed their growth mechanism. By optical evaluation, we found that the InGaN-based high-density nanoumbrella arrays can potentially be used as white LEDs without phosphors. Generally, white LEDs are realized by the combination of GaN-based LEDs with blue light and the phosphors emitting yellow, red and green light. Although research on improving the optical properties and crystal quality of phosphors and lowering the cost of white LEDs with phosphors has been reported,[24] using phosphors increases the cost of white LEDs owing to the need to include a rare-earth element, limiting the efficiency of white LEDs in principle. The reported nanoumbrellas can potentially overcome these issues.

EXPERIMENTAL PROCEDURES

The procedure used to fabricate the high-density arrays of InGaN nanoumbrellas is shown in Figure 1. We employed N-polarity GaN grown on a (0001) sapphire substrate by RF-MBE as a substrate. GaN-based crystals grown by MBE techniques have been investigated.[25,26] In our RF-MBE, Ga and In were supplied from conventional effusion cells using elemental metal sources (7N). The active nitrogen beam was supplied by an RF-plasma source (13.56 MHz) with highly pure nitrogen gas (99.9999%). The substrate was heated from the back side by a resistance-heating element with tantalum (Ta) wires. Then, a Ti layer with ~300 nm thickness was evaporated on the back side of the substrate by electron beam deposition as a heat absorber. The growth temperature was measured by an optical pyrometer. A Ti film with a thickness of 4 nm was also evaporated on the substrate by electron beam deposition. The surface of the substrate containing the Ti film was nitrided via irradiation with an active nitrogen beam at a substrate temperature of ~400 °C, where the RF input power and nitrogen flow rate were 450 W and 3.5 sccm, respectively. Subsequently, Ga and active nitrogen beams were supplied to the surface by RF-MBE at a substrate temperature of 900 °C for 3 h, resulting in the growth of
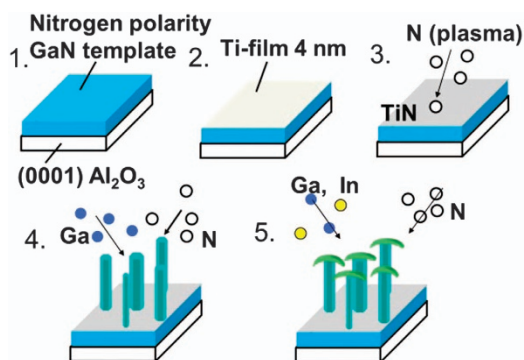
GaN nanocolumns. In the growth, the Ga beam equivalent pressure was 5×10^{-4} Pa. Note that this value was immediately measured below the substrate by a nude ion gauge. In addition, the RF input power and nitrogen flow rate were 450 W and 1.0 sccm, respectively. Next, Ga, In and N plasma were supplied to the surface by RF-MBE at a substrate temperature of 650 °C for 9 min, causing bent InGaN nanoplates to grow on top of the GaN nanocolumns. In the growth, the Ga and In beam equivalent pressures were 5×10^{-5} and 4×10^{-4} Pa, and the RF input power and nitrogen flow rate were 450 W and 1.0 sccm, respectively.
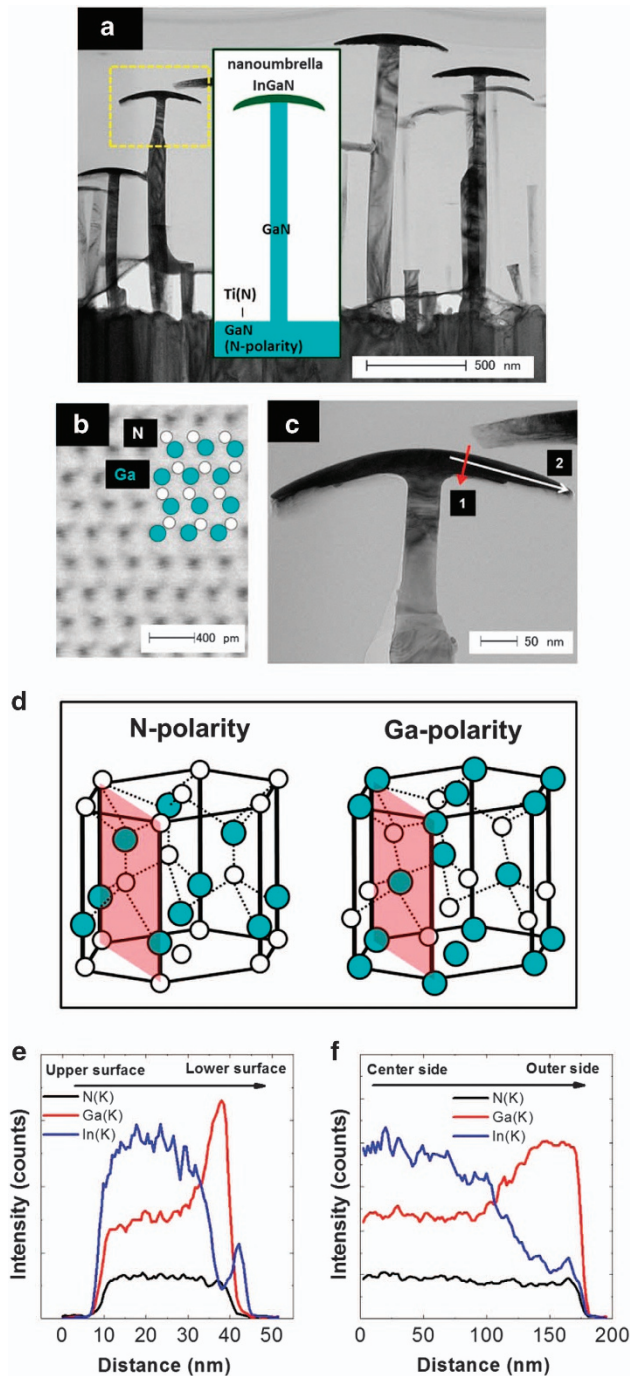
RESULTS AND DISCUSSION

Figure 2 shows scanning electron microscopy images of the fabricated nanocrystals. The nanocrystal exhibits umbrella-like shapes because of the bending of the InGaN nanoplates on top of the GaN nanocolumns. Therefore, we refer to the nanocrystals as InGaN nanoumbrellas. The density of InGaN nanoumbrellas in the array shown in Figures 2a and b is ~8×10^{8} nanoumbrellas per cm². As shown in Figures 2c and d, the hexagonal crystallites that form the bending InGaN nanoplates are all aligned in the same direction, indicating that the crystallites are templated by the underlying N-polarity GaN layer. This suggests that the GaN nanocolumns of the nanoumbrellas began to grow on pits in the nitride-Ti film.

Figure 3 shows typical TEM images and characterization results. As shown in Figure 3a, the diameters and heights of the supporting GaN nanocolumns were ~50–300 nm and 750–1500 nm, respectively. As shown in Figures 2c and 3a, the diameters and thicknesses of the bending InGaN nanoplates were ~200–700 nm and 20–50 nm, respectively. A variety of nanoumbrella configurations were observed in the array. Figure 3b shows a bright-field scanning TEM image of a GaN nanocolumn supporting bending nanoplates. The azimuthal incidence angle was [11–20]. Figure 3d shows the arrangements of Ga and N atoms in the N-polarity and Ga-polarity GaN crystals. The arrangements of Ga and N in the supporting GaN nanocolumn (Figure 3b) agree well with those in the N-polarity GaN crystal. Thus, the supporting GaN nanocolumns have N-polarity, and the crystallites
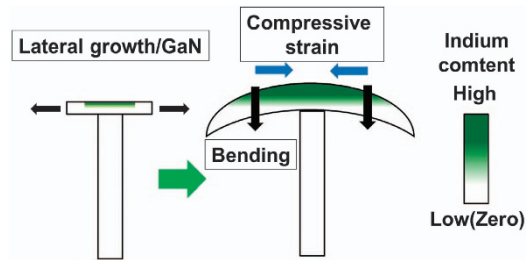

Figure 1 Schematic illustration of the nanoumbrella fabrication procedure.
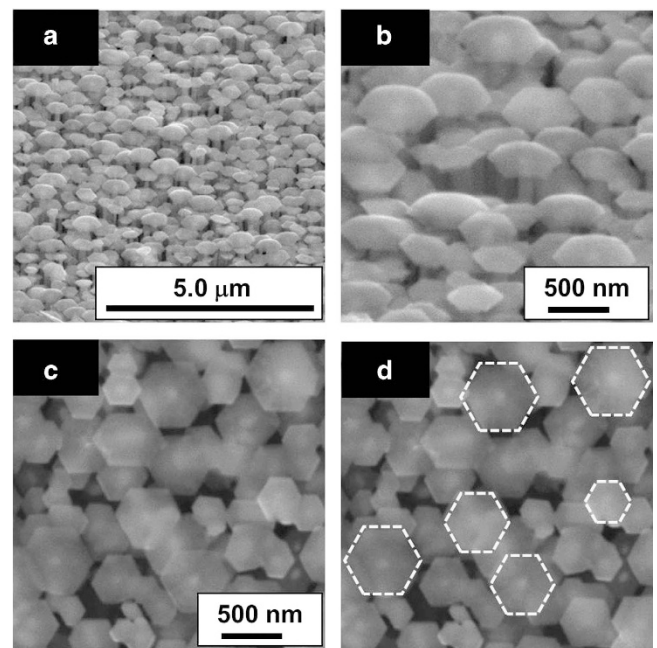
Figure 2 Scanning electron microscopy (SEM) images of the nanoumbrellas: (**a**, **b**) bird's-eye view (tilt angle of 55°) images; (**c**) top-view image; and (**d**) top-view image with highlighted contours.

Figure 4 Schematic illustration of the In distribution in a bending InGaN nanoplate and its growth mechanism.

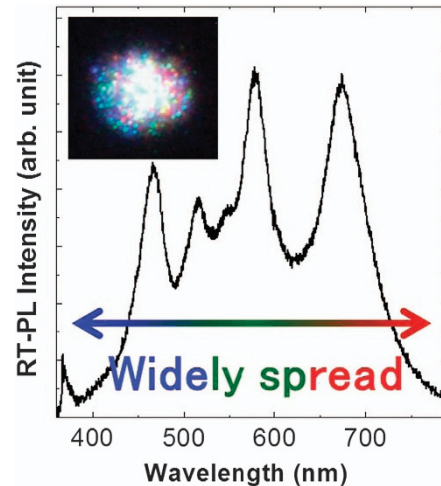

Figure 3 (a) Cross-sectional transmission electron microscopy (TEM) image of InGaN nanoumbrellas (inset: schematic illustration of a nanoumbrella). (b) Bright-field scanning TEM image of a GaN nanocolumn supporting a nanoplate. (c) Magnified TEM image of the nanoplate surrounded by a dashed yellow square in the TEM image shown in (a). (d) Schematic illustration of the arrangements of Ga and N atoms in the N-polarity and Ga-polarity GaN crystals. Energy-dispersive X-ray spectroscopy (EDX) line-scan analyses of the elemental spatial distributions of In, Ga and N along the directions of the (e) red and (f) white arrows in (c).
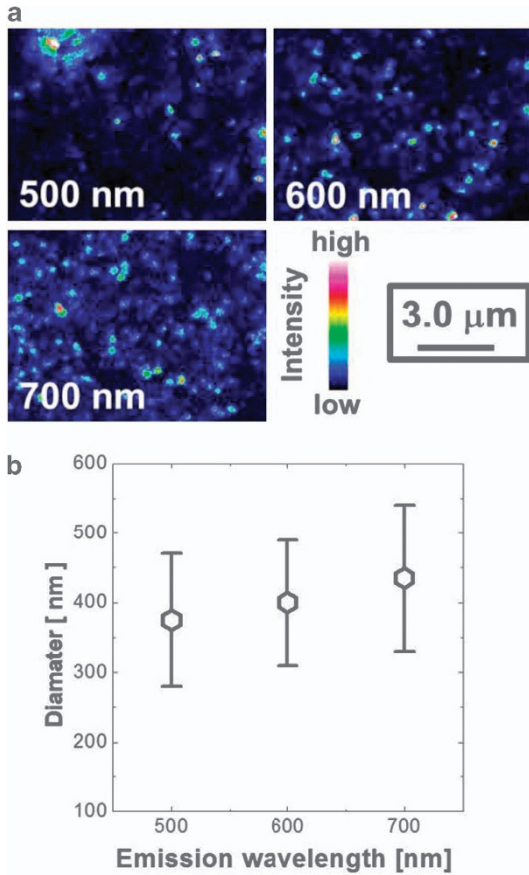

Figure 5 Typical room temperature photoluminescence (RT-PL) spectrum obtained from the high-density nanoumbrella array. The inset shows the RT-PL image excited by the He–Cd laser.

Ti holes may be easily opened up on the Ti film owing to the rough surface. The GaN growth started from the Ti holes, rather than the Ti film. As a result, SAG was realized easily without patterning via electron beam lithography. The growth mechanism has been discussed in detail in previous studies.[1,12,13] Note that these nanocrystals could not be fabricated by crystal growth without the Ti film, namely the growth directly on the N-polarity GaN layer did not realize such nanocrystals. In addition, the TEM images suggested that the supporting GaN nanocolumns of the nanoumbrellas did not include dislocations such as those reported for Ga-polarity GaN nanocolumns.[1] This suggests that the N-polarity GaN nanocolumns consisted of high-quality GaN crystals.

Figure 3c shows a magnified TEM image of the nanoplate surrounded by the dashed yellow square in Figure 3a. The energy-dispersive X-ray spectroscopy line-scan analyses of the spatial distributions of In, Ga and N along the directions of the red and white arrows in Figure 3c are shown in Figures 3e and f, respectively. As shown in Figure 3e, the In content in the middle and upper parts of the nanoplate was higher than that in the lower part. As shown in Figure 3f, the In content gradually decreased toward the edge of the InGaN nanoplate. On the basis of the energy-dispersive X-ray spectroscopy results, a schematic illustration of the In distribution in a bending InGaN nanoplate is shown in Figure 4, and the bending configuration and growth mechanism are discussed in terms of this distribution. The a-axis lattice constants of GaN and InN are 0.319 and 0.355 nm, respectively, and the a-axis lattice constant of InGaN increases with increasing In content. Subsequently, the upper part of

assume the crystalline direction of the underlying N-polarity GaN layer, as mentioned above. We speculate that the rough surface of the N-polarity GaN layer shown in Figure 3a and the Ti film mask produced many points for the initiation of crystal growth. Namely,

Figure 6 (**a**) Cathodeluminescence (CL) images of the same area of the top surface of nanoumbrellas. The inset values (500, 600 and 700 nm) show the wavelength of the emission intensity. (**b**) Relationship between the diameter of the nanoplate and emission wavelength.

the nanoplate was subjected to compressive strain along the a-axis from the lower part, resulting in the bend shown in Figure 4. The bending nanoplates were clearly grown via lateral growth. The edge side of the nanoplate, which had a low In content and a high Ga content, is considered to be the growth surface. This indicates that lateral growth of the GaN crystal mainly contributed to the formation of the bending InGaN nanoplates; in other words, the growth of GaN crystals at a low temperature of 650 °C leads to the formation of the peculiar umbrella-like structures. Therefore, we speculate that the bending InGaN nanoplates were realized by the following two-step growth process: (1) lateral growth of GaN to form the nanoplate and (2) growth of the InGaN crystal on the GaN nanoplate. In this process, the In content of the bending InGaN nanoplate changes as the nanoplate diameter changes. The relationship between the nanocrystal size and the In content has been discussed elsewhere,[15] and the relationship in this case will discussed later in this report.

The photoluminescence (PL) properties of the high-density InGaN nanoumbrella array were characterized at room temperature (RT). Figure 5 shows a typical RT-PL spectrum obtained from the nanoumbrella array; the inset image is the RT-PL image. For the PL characterization, we used a He–Cd laser (continuous wave at a wavelength of 325 nm) as the excitation source. The excitation laser was focused onto a spot using an objective lens of a microscope. The diameter and power density of the excitation spot was $\sim 10 \, \mu m$ and $10 \, W \, cm^{-2}$, respectively. Then, the RT-PL was collected by a bundled
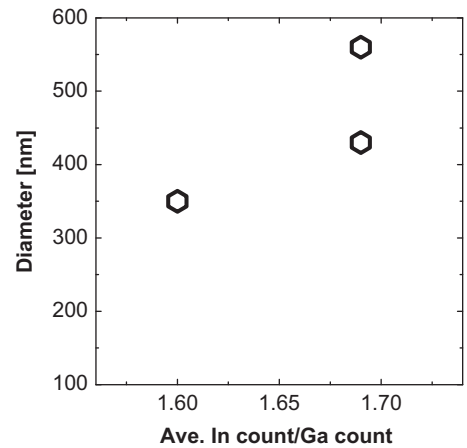

Figure 7 Relationship between the diameter of the nanoplate and average In count/Ga count ratio near center side of the nanoplate obtained by energy-dispersive X-ray spectroscopy (EDX) line-scan analysis.
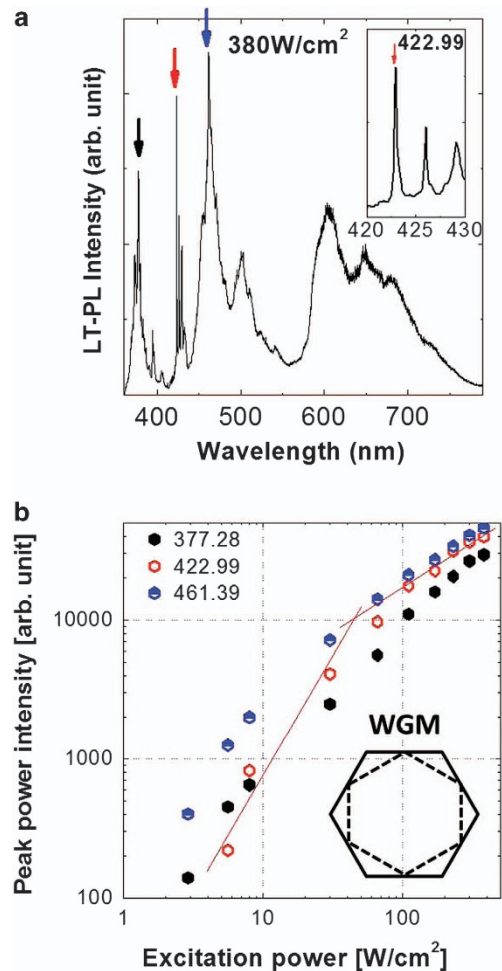
Figure 8 (**a**) Typical low-temperature (LT; 4 K) photoluminescence (PL) spectrum obtained from the high-density nanoumbrella array. (**b**) PL peak intensities at 377.28, 422.29 and 461.39 nm plotted as a function of the excitation power density.

fiber with the same objective lens, and the bundled fiber was connected to a spectrometer with a charge-coupled device array detector. The objective lens was provided just above the top surface
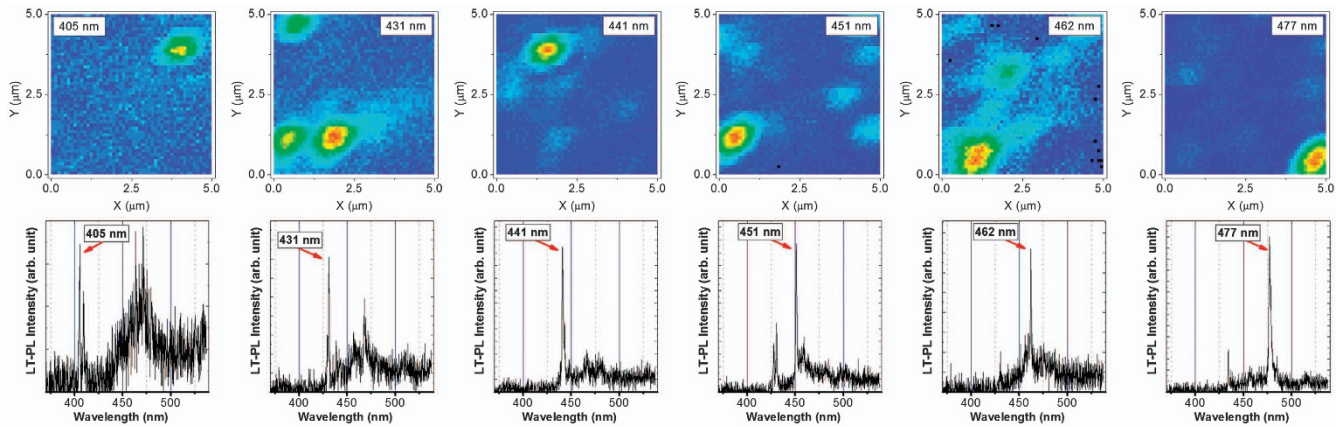
Figure 9 Mapping images of the intensities at the wavelengths of the sharp peaks (the wavelength is shown in each figure) and the spectra showing the highest intensity at the wavelengths.

of the sample. As shown in Figure 5, the wavelength range of the emission spectrum obtained from the nanoumbrella array was extremely wide ($\sim$360–800 nm); thus, the spectrum covered the entire visible-light region. As shown in the inset image of Figure 5, many bright spots with various colors were observed. These spots likely originated from the bending InGaN nanoplates of the nanoumbrellas. Namely, the emission of different wavelengths of light by the bending InGaN nanoplates in the array contributed to the extremely wide wavelength range of the emission spectrum, similar to that of white light. Importantly, the white light emission was obtained from an extremely small area with a diameter of $\sim$10 μm. As mentioned above, the various emissions were probably caused by the nonuniform configurations of the bending nanoplates. To the best of our knowledge, such a wide range of emission wavelengths obtained from a small-diameter source has not previously been achieved by InGaN-based nanocrystals fabricated via self-assembly and SAG techniques.

We investigated the factor causing the color variation (as shown in Figure 5) by cathodeluminescence evaluation. Figure 6a shows cathodeluminescence images of the top view of the high-density nanoumbrella array for emission with different wavelengths. Note that the three images shown in Figure 6a were obtained from the same observation area. As shown in Figure 6a, the points producing strong emission varied with the wavelength. Then, by comparing the cathodeluminescence and scanning electron microscopy images of the observation area, we could clarify the relationship between the emission color and diameter of the nanoplate of the nanoumbrellas, as shown in Figure 6b. We found a trend that the wavelength of the emission redshifted with increasing diameter of the nanoplates of the nanoumbrellas. We also performed additional energy-dispersive X-ray spectroscopy line-scan analyses of the spatial distributions of In, Ga and N for other nanoplates of the nanoumbrellas with diameters of 350 and 560 nm by the same technique as for in Figures 3c and f. These results also showed almost the same trend; the In content gradually decreased toward the edge of the InGaN nanoplate and the decrease started at a distance of $\sim$100 nm from the edge, as shown in Figure 3f. On the basis of the results, we estimated the average the In count/Ga count ratio near the center of the nanoplates, as shown in Figure 7. The In content increased with increasing the nanoplate diameters. This result is consistent with the cathodeluminescence results shown in Figure 6. Consequently, the factor causing the color variation was probably the diameter of the nanoplate.

We also characterized the PL properties of the high-density InGaN nanoumbrella array at a low temperature of 4 K using a continuous-wave laser with a wavelength of 266 nm (frequency-doubled 532 nm laser (Verdi-G18, Coherent, Santa Clara, CA, USA)) as the excitation source. The excitation laser was focused onto a spot using an objective lens of a microscope, and the diameter of the excitation area was $\sim$3.0 μm. Note that the PL evaluation system was almost the same as previously described except for the excitation laser. Figure 8a shows a typical low-temperature-PL (LT-PL) spectrum obtained from the high-density InGaN nanoumbrella array; the inset figure shows a magnified view of the spectrum at $\sim$420 nm. Multiple sharp peaks were observed in the spectrum in the wavelength range of $\sim$360–500 nm. For example, the full width at half maximum of the sharp peak at 422.99 nm was 0.3 nm. The intensities of these sharp peaks increased nonlinearly with increasing excitation power, as shown in Figure 8b; the threshold power densities were <10 W cm^{-2}. Therefore, we concluded that the sharp peaks likely indicated lasing actions. In nanocrystals and nanocrystal arrays, the optical cavities of the photonic crystals, random lasing actions and the WGM have been demonstrated. Generally, the photonic crystal effect cannot be exhibited in an array because of its low periodicity. According to previous reports, the peak wavelengths of the random lasers are not temporally stable.[27–29] The peaks in Figure 8a were not temporally invariable, and the peaks were not considered to be based on a random laser. In many previous reports, the WGM acted as the optical resonant mode in hexagonal nano- and microcrystals.[21–23] We also demonstrated lasing action in a single hexagonal GaN nanodisk.[19] Thus, it is reasonable to attribute the sharp peaks and lasing action to the WGM in a bending nanoplate (Figure 8b).

We investigated the properties of the sharp peaks in the LT-PL spectra in detail using an excitation spot with a diameter of $\sim$400 nm and an excitation power density of 12 W cm^{-2}. The extremely small diameter of the excitation spot was adjusted by lenses and spatial filters. Using the extremely small excitation spot, we can evaluate the optical properties of only one or two nanoumbrellas in the array, and we produced LT-PL mapping images of the high-density InGaN nanoumbrella array with an area of 5×5 μm^2. In the experiment, the LT-PL spectra were corrected while the excitation spot was moved by moving the objective lens in 100 nm steps using the piezo stages. Figure 9 shows the mapping images of the intensities at the wavelengths of the sharp peaks (the wavelength is shown in each figure) and the spectra showing the highest intensity at the wavelengths, where observation areas were the same. As shown in Figure 9, sharp peaks at the specific wavelengths were obtained from the localized area, indicating that one or two nanoumbrellas
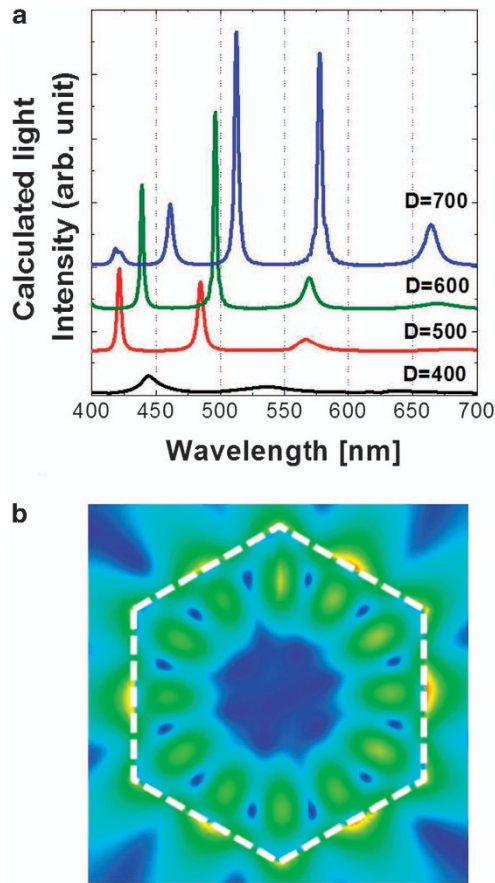
Figure 10 (**a**) Two-dimensional finite difference time domain (2D-FDTD) calculated light response spectra for the whispering gallery mode (WGM) in hexagons with diameters of 400, 500, 600 and 700 nm. (**b**) 2D-FDTD calculated electric field distribution of standing wave in a hexagon with a diameter of 600 nm at a specific wavelength of 496.1 nm.

contributed to the sharp peak. Thus, the sharp peaks were not caused by random lasing action or the photonic crystal effect.

We also investigated the WGM property in a hexagon with a diameter of 200–700 nm by a numerical analysis using the two-dimensional finite difference time domain method for the transverse electric mode; the electric fields polarized along the top surface of the hexagon (GaN-based crystals dominantly exhibit transverse electric-mode optical gain). In the calculation, white light impulse plane waves are generated in a hexagon, and the light signal is collected and the signal is Fourier transformed. The refractive index of GaN is well known to be ~ 2.4–2.5 in the visible region. However, we cannot use reference refractive indices for the InGaN crystals with various In contents. The refractive index of the hexagon was assumed to be 2.5; we consider that this value is reasonable for investigating the trend of the WGM property in a hexagon. In the calculation, we simply examine the trend of the WGM properties, and the precise peak positions and other details of the WGM are not discussed. Figures 10a and b show the two-dimensional finite difference time domain calculated light response spectra for the WGM in hexagons with various diameters and the calculated electric field distributions of standing waves at a resonant light of 496.1 nm wavelength in a hexagon of 600 nm diameter, respectively. When the diameter is more than ~ 350 nm, resonant peaks are obtained in the light response spectra as shown in Figure 10a, and the distributions of the standing

waves at the resonant peaks are similar to that of the WGM as shown in Figure 10b. However, we cannot obtain such resonant peaks from a hexagon with a diameter of less than ~ 350 nm. In addition, the resonant peaks markedly decrease in intensity above a wavelength of 600 nm for the hexagons with diameters of 400–700 nm. The behaviors are probably caused by the wavelength being too long to oscillate in the hexagon owing to its size. The calculated results indicate that the InGaN-based nanoplates with a diameter of ~ 400–700 nm potentially act as WGM resonators up to a wavelength of ~ 600 nm. The calculated results also indicate that GaN nanocolumns with a diameter of ~ 50–300 nm of the nanoumbrellas cannot act as WGM resonators. Furthermore, nonsharp peaks were experimentally observed in the wavelength range of ~ 550–750 nm, and the experimental finding were well explained by the finite difference time domain results in addition to the experimental results that the In contents of the edge side of the bending InGaN nanoplates were low; the resonant light of the WGM localizes at the edge side of the bending InGaN nanoplates, as shown in Figure 10b. Note that further analysis and other approaches are required to clarify the resonant system in terms of the WGM in the nanosize hexagon, but the results indicate that hexagons with such diameters act as WGM resonators.

As mentioned above, the InGaN-based nanoumbrella arrays having a limited microsize area exhibited a wide range of emissions and good color-rendering properties, indicating that white LEDs can be realized without phosphors. In addition, it is remarkable that each isolated nanoumbrella potentially exhibited lasing action based on the WGM, indicating that each isolated nanoumbrella potentially acts as a laser diode with high efficiency. Thus, we consider that the high-density InGaN-based nanoumbrella array can be potentially used as a high-efficiency novel white light source without phosphors.

CONCLUSION

We fabricated a high-density nanoumbrella array on a N-polarity GaN template coated by a thin Ti layer via RF-MBE crystal growth. Crystal structure characterization by TEM indicated that the nanoumbrellas consisted of high-quality N-polarity GaN-based crystals, and the growth mechanism of the nanoumbrellas was discussed. However, clarifying the details of the growth mechanism of the peculiar nanoumbrella structure will require further investigation. Optical evaluation demonstrated that the high-density nanoumbrella array exhibited an extremely wide range of emission wavelengths resembling white light from a small excitation area of $\sim 10 \, \mu m^2$. In addition, multiple lasing actions and resonant peaks are considered to have been observed in the LT-PL spectrum. The optical cavities were likely caused by a WGM in a single bending InGaN nanoplate. The optical properties of the high-density InGaN-based nanoumbrella array suggest its potential use in high-performance novel white LEDs and laser diodes without phosphors.

CONFLICT OF INTEREST

The authors declare no conflict of interest.

1 Kishino, K. & Ishizawa, S. Selective-area growth of GaN nanocolumns on Si(111) substrates for application to nanocolumn emitters with systematic analysis of dislocation filtering effect of nanocolumns. *Nanotechnology* **26**, 225602 (2015).

2 Zhu, J. H., Wang, L. J., Zhang, S. M., Wang, H., Zhao, D. G., Zhu, J. J., Liu, Z. S., Jiang, D. S. & Yang, H. Light extraction efficiency improvement and strain relaxation in InGaN/GaN multiple quantum well nanopillars. *J. Appl. Phys.* **109**, 084339 (2011).

3 Kikuchi, A., Yamano, K., Tada, M. & Kishino, K. Stimulated emission from GaN nanocolumns. *Phys. Stat. Sol.* **241**, 2754 (2004).

4 Yoshizawa, M., Kikuchi, A., Mori, M., Fujita, N. & Kishino, K. Growth of self-organized GaN nanostructures on Al2O3(0001) by RF-radical source molecular beam epitaxy. *Jpn. J. Appl. Phys.* **36**, L459 (1997).

5 Kikuchi, A., Tada, M., Miwa, K. & Kishino, K. Growth and characterization of InGaN/GaN nanocolumn LED. *Proc. SPIE* **6129**, 612905 (2006).

6 Johnson, J. C., Choi, H. J., Knutsen, K. P., Schaller, R. D., Yang, P. & Saykally, R. J. Single gallium nitride nanowire lasers. *Nat. Mater.* **1**, 106 (2002).

7 Choi, H. J., Johnson, J. C., He, R. R., Lee, S. K., Kim, F., Pauzauskie, P., Goldberger, J., Saykally, R. J., & Yang, P. J. Self-organized GaN quantum wire UV lasers. *Phys. Chem. B* **107**, 8721 (2003).

8 Kikuchi, A., Kawai, M., Tada, M. & Kishino, K. InGaN/GaN multiple quantum disk nanocolumn light-emitting diodes grown on (111)Si substrate. *Jpn. J. Appl. Phys.* **43**, L1524 (2004).

9 Kim, H. M., Cho, Y. H., Lee, H., Kim, S.I., Ryu, S. R., Kim, D. Y., Kang, T. W., & Chung, K. S. High-brightness light emitting diodes using dislocation-free indium gallium nitride/gallium nitride multiquantum-well nanorod arrays. *Nano Lett.* **4**, 1059 (2004).

10 Ristic, J., Calleja, E., Femanedez-Garrido, S., Trampert, A., Jahn, U., Ploog, K. H., Povoloski, M., & Di Carlo, A. GaN/AlGaN nanocavities with AlN/GaN Bragg reflectors grown in AlGaN nanocolumns by plasma assisted MBE. *Phys. Stat. Sol. A* **202**, 367 (2005).

11 Kouno, T., Kikuchi, A. & Kishino, K. Growth of high-In-content InGaN multiple quantum disk nanocolumns on Si(111) by RE plasma-assisted molecular-beam epitaxy. *Phys. Stat. Sol. B* **243**, 7 (2006).

12 Hersee, S. D., Sun, X. Y. & Wang, X. The controlled growth of GaN nanowires. *Nano Lett.* **6**, 1808 (2006).

13 Sekiguchi, H., Kishino, K. & Kikuchi, A. Ti-mask selective-area growth of GaN by RF-plasma-assisted molecular-beam epitaxy for fabricating regularly arranged InGaN/GaN nanocolumns. *Appl. Phys. Express* **1**, 124002 (2008).

14 Kouno, T., Kishino, K., Yamano, K. & Kikuchi, A. Two-dimensional light confinement in periodic InGaN/GaN nanocolumn arrays and optically pumped blue stimulated emission. *Opt. Express* **17**, 20440 (2009).

15 Sekiguchi, H., Kishino, K. & Kikuchi, A. Emission color control from blue to red with nanocolumn diameter of InGaN/GaN nanocolumn arrays grown on same substrate. *Appl. Phys. Lett.* **96**, 231104 (2010).

16 Kouno, T., Kishino, K., Suzuki, T. & Sakai, M. Lasing action in GaN tiny hexagonal nanoring resonators. *IEEE Photonics J.* **6**, 1027 (2010).

17 Albert, S., Bengoechea-Encabo, A., Sanchez-Garcia, M. A., Calleja, E. & Jahn, U. Selective area growth and characterization of InGaN nanocolumns for phosphor-free white light emission. *J. Appl. Phys.* **113**, 114306 (2013).

18 Son, J. S., Honda, Y., Yamaguchi, M. & Amano, H. Characterization of nonpolar a-plane InGaN/GaN multiple quantum well using double nanopillar SiO2 mask. *Jpn J. Appl. Phys.* **53**, 05FL01 (2014).

19 Kouno, T., Sakai, M., Kishino, K. & Hara, K. Light confinement in hexagonal GaN nanodisk with whispering gallery mode. *Jpn J. Appl. Phys.* **53**, 068005 (2014).

20 Kouno, T. & Kishino, K. Well-arranged novel InGaN hexagonal nanoplates at the tops of nitrogen-polarity GaN nanocolumn arrays. *AIP Advances* **2**, 012140 (2012).

21 Nobis, T., Kaidashev, E. M., Rahm, A., Lorenz, M. & Grundman, M. Whispering gallery modes in nanosized dielectric resonators with hexagonal cross section. *Phys. Rev. Lett.* **93**, 103903 (2004).

22 Wang, D., Seo, H. W., Tin, C. C., Bozack, M. J., Williams, J. R., Park, M. & Tzeng, Y. Lasing in whispering gallery mode in ZnO nanonails. *J. Appl. Phys.* **99**, 093112 (2006).

23 Gargas, D. J., Moore, M. C., Ni, A., Chang, S. W., Zhang, Z., Chuang, S. L. & Yang, P. Whispering galley mode lasing from zinc oxide hexagonal nanodisks. *ACS NANO* **4**, 3270 (2010).

24 Ye, S., Xiao, F., Pan, Y. X., Ma, Y. Y. & Zhang, Q. Y. Phosphors in phosphor-converted white light-emitting diodes: recent advances in materials, techniques and properties. *Mater. Sci. Eng. R Rep.* **71**, 1 (2010).

25 Moustakas, T. D., Lei, T. & Molnar, R. J. Growth of GaN by ECR-assisted MBE. *Physica B* **185**, 36 (1993).

26 Lin, M. E., Sverdlov, G. L., Zhou, G. L. & Morkoc, H. A comparative study of GaN epilayers grown on sapphire and SiC substrates by plasma-assisted molecular-beam epitaxy. *Appl. Phys Lett.* **62**, 3479 (1993).

27 Sakai, M., Inose, Y., Ema, K., Ohtsuki, T., Sekiguchi, H., Kikuchi, A., & Kishino, K. Random laser action in GaN nanocolumns. *Appl. Phys. Lett.* **97**, 151109 (2010).

28 Yu, S. F., Yuen, C., Lau, S. P., Park, W. I. & Yi, G.-C. Random laser action in ZnO nanorods arrays embedded in ZnO epilayers. *Appl. Phys. Lett.* **84**, 3241 (2004).

29 Nakamura, T., Hosaka, T. & Adachi, S. Gold-nanoparticle-assisted random lasing from powdered GaN. *Opt. Express* **19**, 467 (2011).